



Molecular Dynamics Simulation of the Nanofluidic Energy Absorption System Under Mid-speed Loading

Sayed Hossein Ganjiani¹ · Alireza Hossein Nezhad¹

Received: 2 October 2016 / Accepted: 15 June 2018 / Published online: 20 June 2018
© Shiraz University 2018

Abstract

In this work, a nanofluidic energy absorption system (NEAS) under mid-speed loading is investigated by using molecular dynamics simulation. Usually, two types of dynamic and quasi-static loadings have been applied on NEAS. In the dynamic loadings, NEAS is taken under high-speed loadings in the range of 5 m/s up to 1000 m/s, and in the quasi-static loadings, it is taken under low-speed loadings in the range of less than or equal to 0.0005 m/s. Here, to investigate the performance of NEAS under mid-speed loading, four loading rates of 0.2, 0.4, 0.8 and 1.0 m/s are considered. Also, four armchair CNTs (8,8), (10,10), (12,12) and (14,14) were selected to study the effects of nanotube size. The results of simulations showed that contact angle which shows the hydrophobicity of carbon nanotube (CNT) is reduced on average 3.6% by increasing the loading rate in all CNTs, leading to an average 41.7% decrease of infiltration pressure and an average 16% reduction of absorbed energy density in all CNTs. No friction is observed at the loading rate of 0.2 m/s in all CNTs during movement of water molecules in CNT. But, at the other loading rates, friction is increased by increasing the loading rate, leading to an average 24.8% reduction of the absorbed energy efficiency of NEAS in all CNTs. Also, contact angle, infiltration pressure, absorbed energy density and efficiency are decreased by increasing the CNT diameter.

Keywords Carbon nanotube · Infiltration pressure · Loading rate · Surface tension · Friction

1 Introduction

NEAS has been highly desirable due to high efficiency of absorbed energy. In this system, a large number of hydrophobic nanoporous particles are mixed in the functional liquids. Initially, liquid molecules cannot enter into the nanopores of nanoporous particles. If liquid–nanoporous particles are kept under pressure, a large number of liquid molecules infiltrate the nanopores after the pressure of system reaching to a threshold pressure (infiltration pressure). In NEAS, an energy conversion is occurred through solid–liquid interface in nanopores. A part of input mechanical energy is stored by surface tension and the other part is converted into heat by friction (Chen et al. 2014). NEAS can be put under a wide range of loading rates, and it can be used in different applications such as

damper. Since the amount of damping produced in a damper is proportional to velocity, it is important to understand the effect of all range of load speeds on a NEAS.

NEAS has been studied by experimental (Han et al. 2006, 2008, 2009; Han and Qiao 2007; Qiao et al. 2008; Surani et al. 2005; Kong and Qiao 2005) and simulation (Xu et al. 2011; Liu et al. 2008, 2009; Liu and Cao 2014) works. The effects of different parameters such as nanopores size and geometry (Liu et al. 2009; Xu et al. 2011), temperature (Xu et al. 2011; Liu et al. 2009), type of liquid (Kong and Qiao 2005; Liu and Cao 2014), type of nanoporous materials (Han et al. 2009), electrical charge (Liu et al. 2008), electrical field (Xu et al. 2011) and ion concentration (Kong and Qiao 2005) have been investigated on the characteristic performance of NEAS such as infiltration pressure, absorbed energy density and efficiency. Depending on various applications, two types of quasi-static (Qiao et al. 2008; Han et al. 2006; Liu et al. 2009; Xu et al. 2011) and dynamic (Surani et al. 2005; Liu and Cao 2013, 2014; Cao 2012; Xu et al. 2014) loadings are applied

✉ Alireza Hossein Nezhad
nezhadd@hameen.usb.ac.ir

¹ Department of Mechanical Engineering, University of Sistan and Baluchestan, Zahedan, Iran

on NEAS. In cases such as damping or vibration proof, the speed and amount of loading are relatively low; thus, quasi-static loading is applied. But in cases such as blast protection, car bumper and body armor, the speed and amount of loading are high, so dynamic loading is applied. A loading–unloading cycle is applied on NEAS in simulation and experimental works in which quasi-static loading is investigated. System is at equilibrium at all steps of loading and unloading processes. In this type of loading, pressure variations versus infiltrated liquid volume have a hysteresis curve. Depending on the types of liquid and solid phases, if surface tension overcomes friction then water molecules defiltrate from nanopores after unloading process (Kong and Qiao 2005), but otherwise water molecules stay in nanopores (Qiao et al. 2008). System does not return to initial state and will not be used again if water molecules do not leave nanopores. A mechanical wave is created in dynamic loading due to high loading rate. The mechanical wave moves to the end of nanopores and then back. Loading rate in dynamic loading is at the order of 5 m/s up to 1000 m/s (Cao 2012; Xu et al. 2014). Effects of loading rate have been investigated in dynamic loading (Liu and Cao 2013). In dynamic loadings, infiltration pressure and absorbed energy efficiency are increased by increase of loading rate (Surani et al. 2005; Zhao et al. 2009). The free energy difference between the water molecules inside and outside of the CNT causes the infiltration in quasi-static loading, while in the dynamic loading, the infiltration of the water molecules in the CNT occurs by external work (Cao et al. 2008).

Loading rates are classified as low, medium and high. The minimum reported loading rate at high-speed loading is 5 m/s (Zhao et al. 2009); the effects of dynamic loading are weak and can be considered as quasi-static loading. The effects of loading rate in quasi-static loading have been studied only in experimental works. The maximum reported loading rate in low-speed loading is 0.0005 m/s (Han et al. 2008). Although mid-speed loadings have more applications in damping systems, according to the best of the author's knowledge, NEAS performance has not been investigated so far for these loadings. Therefore, in this paper, the effects of loading rate in mid-speed loading on the performance characteristics of NEAS such as infiltration pressure, absorbed energy density, radial density profile and absorbed energy efficiency are investigated.

2 Model and Computational Method

2.1 Computational Model

Computational model includes a rigid CNT and a rectangular reservoir as shown in Fig. 1. Reservoir is bounded in

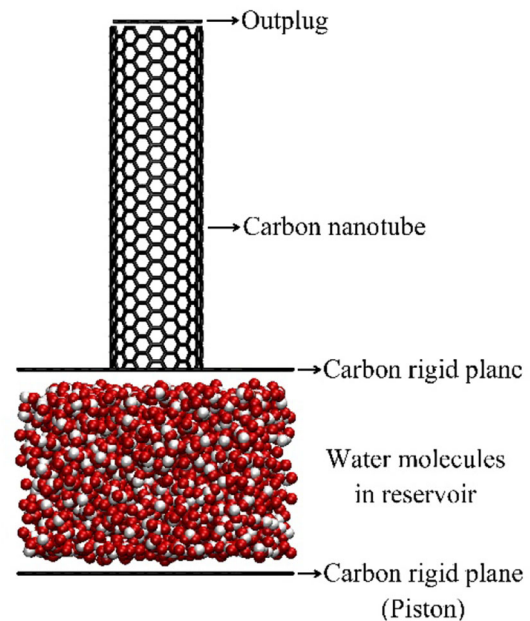


Fig. 1 Computational model. Computational model includes a reservoir and a 5-nm-rigid CNT

the top and the bottom by two rigid graphene planes. The upper plane is fixed and the lower plane which acts like a piston is movable. A CNT is attached to the upper plane and the upper end of the CNT is closed by a rigid graphene plug. Length of CNT is 5 nm. Four armchair CNTs (8,8), (10,10), (12,12) and (14,14) with diameters 1.085, 1.356, 1.627 and 1.898 nm, respectively, are considered. The reservoir dimensions are $34.43 \times 34.79 \times 24.97 \text{ \AA}^3$. 1000 water molecules are considered in the reservoir; as a result, the density of water molecules becomes as 1.0 g/cm^3 , which is equal to the density of bulk water at 300 K and 1 atm.

2.2 Computational Method

The 12-6 Lennard-Jones (LJ) and columbic potentials are used for the interatomic van der Waals (vdW) and electrostatic interactions, respectively (Leach 2011):

$$V(r_{ij}) = \sum_{i=1}^N \sum_{j=i+1}^N \left(4\epsilon_{ij} \left[\left(\frac{\sigma_{ij}}{r_{ij}} \right)^{12} - \left(\frac{\sigma_{ij}}{r_{ij}} \right)^6 \right] + \frac{q_i q_j}{4\pi\epsilon_0 r_{ij}} \right) \quad (1)$$

where r_{ij} is the distance between two atoms i and j , q is the electrical charge of the atom, and ϵ and σ are energy and distance parameters in LJ potential, respectively. The intramolecular bond stretching and angle bending interactions in water molecules are modeled by harmonic potentials (Leach 2011):

$$V(\vec{r}) = \sum_{\text{bonds}} \frac{k_{\text{bond}}}{2} (l_i - l_{i,0})^2 + \sum_{\text{angles}} \frac{k_{\text{angle}}}{2} (\theta_i - \theta_{i,0})^2 \quad (2)$$

where k_{bond} and k_{angle} are coefficients of the harmonic potentials of the bond stretching and angle bending in water molecules, respectively, and l_i and $l_{i,0}$ are the bond length and the reference bond length of O–H bond in the i th water molecules. θ_i and $\theta_{i,0}$ are the angle and the reference angle between two O–H bonds in the i th water molecules. Since flexibility of CNT has no influence on the NEAS performance characteristics (Xu et al. 2011), CNT is assumed as rigid. Therefore, the intramolecular interactions between carbon atoms in CNT are neglected. The TIP3P model is used for water molecules, and carbon–water and carbon–carbon interactions parameters are ($\epsilon_{\text{co}} = 0.06461$ kcal/mol, $\sigma_{\text{co}} = 3.4138$ Å) and ($\epsilon_{\text{cc}} = 0.086$ kcal/mol, $\sigma_{\text{cc}} = 3.40$ Å), respectively (Hummer et al. 2011).

To model a real NEAS, on the four lateral surfaces of the computational model, periodic boundary conditions are applied.

The piston moves in a stepwise manner. After each step of displacement, piston is kept fixed about 50 ps to allow the system to reach equilibrium. To investigate the effects of loading rate, four speeds 0.2, 0.4, 0.8 and 1.0 m/s for piston are considered. The displacement step depends on the piston speed, for example, 0.1 Å at 0.2 m/s. The total displacement of the piston is 10 Å at all loading rates. After piston reaches to the end of the displacement, it returns to its initial position at the same speed of loading rate; as a result, the application of loading–unloading cycle on the system is completed. Before piston starts to move, the CNT opening is kept closed by a lid about 50 ps, in order to allow water molecules to be equilibrated in the reservoir. Then, the lid is removed and the whole system is equilibrated about 50 ps again.

The MD simulation of the infiltration of the water molecules into the CNTs is carried out using LAMMPS code (Plimpton 1995). At all steps, the NVT ensemble with Nose–Hoover thermostat is used to fix temperature at 300 K. The cutoff distance of LJ potential is set to 10 Å. The PPPM method with accuracy of 10^{-4} is used to calculate long-range Columbic potential of water molecules. The time step in all simulations is set to 1 fs.

The pressure in the reservoir can be obtained at all steps in terms of the density by the equation of state (Cao et al. 2008):

$$P = P_0 + 298 \left[\left(\frac{\rho}{\rho_0} \right)^{7.15} - 1 \right] \quad (3)$$

where ρ is density, and ρ_0 and P_0 are initial density and pressure, respectively. The values of ρ_0 and P_0 are taken 1 g/cm³ and 0.1 MPa, respectively. The volume and

number of water molecules in the reservoir change by the piston displacement, and as a result, the density of water molecules in the reservoir will change.

2.3 Simulation Verification

According to the work of Liu et al. (2009), a simulation is performed before investigation of the loading rate effects on the NEAS performance. In this simulation, SPE/C model is used for constants and coefficients in intramolecular interactions in water molecules. The piston speed is 0.1 m/s, and the displacement step is 0.05 Å. The final displacement of piston is 6 Å. Carbon–water interaction parameters are $\epsilon_{\text{co}} = 0.07471$ kcal/mol and $\sigma_{\text{co}} = 3.194$ Å (Bojan and Steele 1987). Other features in the computational model and method are identical to those described in Sects. 2.1 and 2.2. For verification, pressure variations versus the number of infiltrated water molecules in CNT (infiltration curve) in both works are compared in Fig. 2. It is observed that infiltration curves have excellent agreement. The maximum difference between infiltration pressures is less than 1%.

3 Results and Discussions

3.1 Infiltration Pressure

Infiltration pressure is a very important characteristic in NEAS. The infiltration pressure is a pressure inside the system after which water molecules can enter the CNT. The infiltration curves of loading–unloading cycles in different loading rates in (10,10) CNT are shown in Fig. 3. Infiltration curve trends in other CNTs in different loading rates are the same as Fig. 3. In the infiltration curves, water molecules are compressed in the reservoir initially, and

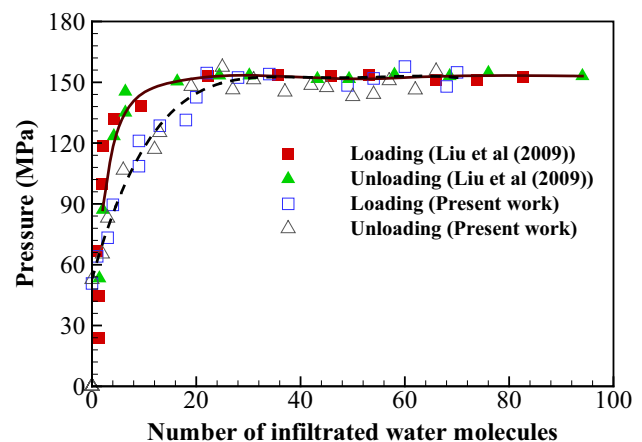


Fig. 2 Comparison infiltration curve obtained from present work with that of Liu et al. (2009)

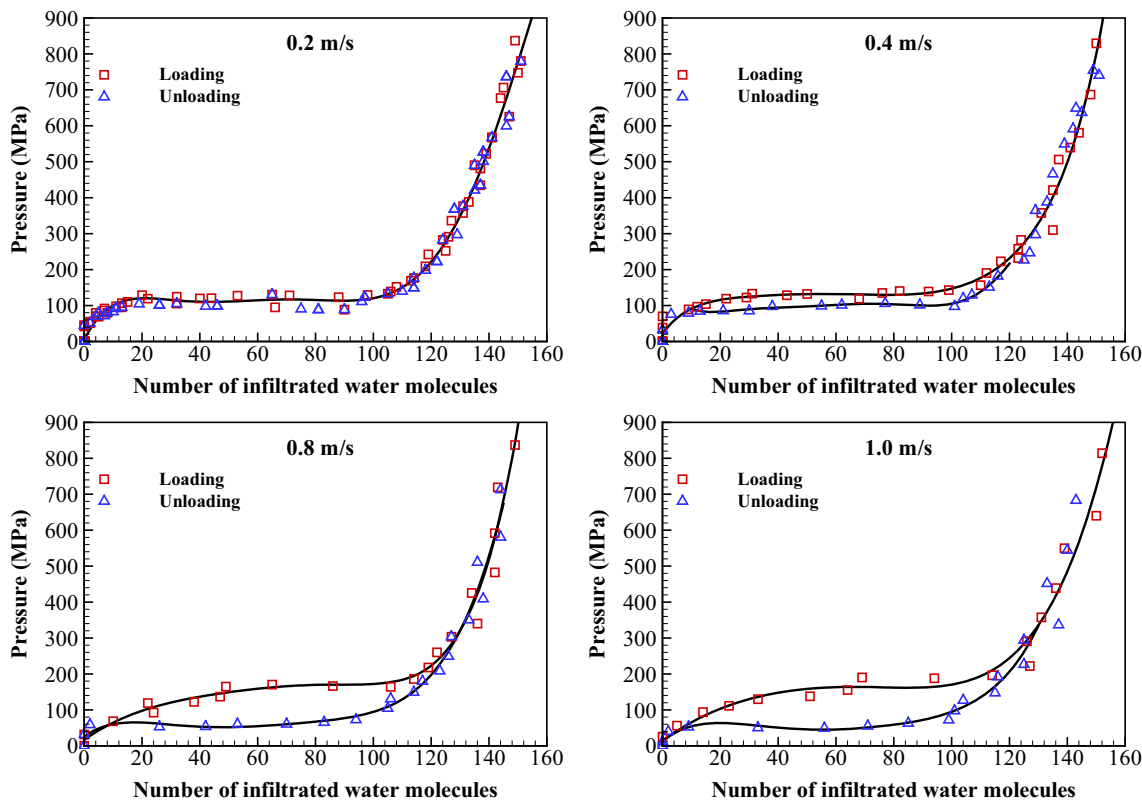


Fig. 3 Infiltration curves at different loading rates in (10,10) CNT

then they enter CNT, after that the pressure of the system reaches the infiltration pressure. The infiltration plateau is formed in the infiltration curve until water molecules reach the end of CNT. After CNT is filled, water molecules are compressed in the reservoir and CNT.

Unloading process is overlapped on loading process only at loading rate of 0.2 m/s. But paths of loading and unloading processes in the infiltration plateau are different at other loading rates. Difference between two paths is increased by increasing the loading rate. Water molecules flow out the CNT entirely at the end of unloading process at all loading rates. Also, the infiltration plateau slope is increased by increasing the loading rate.

Figure 4 shows the variation of infiltration pressure versus loading rate at different CNTs. It is observed that infiltration pressure at different CNTs is decreased by increasing loading rate. Also, infiltration pressure at constant loading rate is decreased by increasing diameter of CNT. Infiltration pressure is decreased on average 41.6% in all CNTs by increasing the loading rate from 0.2 m/s up to 1.0 m/s.

3.2 Radial Density Profile

Radial density profile (RDP) is defined as $g_r = n_r/2\pi r\Delta r n_{in}$, in which n_r is the number of water molecules in a

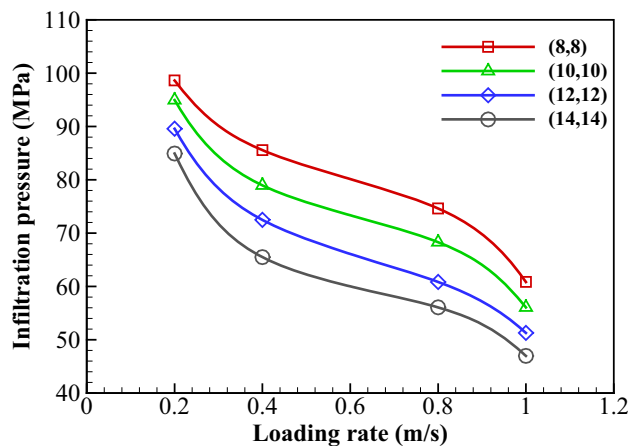


Fig. 4 Variation of infiltration pressure versus loading rate in different CNTs

cylindrical annulus with the inner radius r and thickness Δr , and n_{in} is the number of water molecules in CNT. RDP is used to investigate structure of water molecules in CNT. Figure 5 shows RDP of water molecules in (10,10) CNT at different loading rates. Data is averaged when the piston has moved from 0.8 to 1.0 nm. As shown in Fig. 5, unlike water liquid, RDP is nonuniform in CNT and has two shells: The first shell is near the CNT wall, and the second shell is near the CNT center. For all loading rates, the value

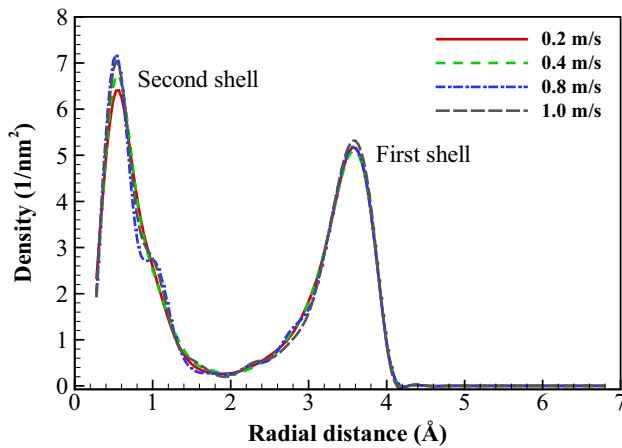


Fig. 5 Radial density profiles at different loading rates

of the RDP in the second shell is more than that in the first shell. This means that water molecules tend to approach the CNT center. The RDPs at all the loading rates are almost identical, except that the value of RDP in the second shell is increased 11% by increasing the loading rate.

3.3 Energy Conversion

Surface tension and friction in processes of infiltration and defiltration affect the motion of water molecules in CNT. If there is friction in CNT, pressure in infiltration plateau will be changed. As shown in Fig. 3, infiltration plateau at loading rate 0.2 m/s is without slope; therefore, there is no friction in CNT in this situation.

In experimental works (Qiao et al. 2008; Han et al. 2008), there is a distribution of CNT size. Infiltration pressure is decreased by increasing CNT size (Liu et al. 2009). Therefore, in addition to friction, a distribution of infiltration pressure causes the infiltration plateau to have a slope in nanoporous materials. But, there is one CNT in this work; therefore, slope of infiltration plateau is caused by friction in loading rates from 0.4 to 1.0 m/s.

Friction in CNT is increased by increasing the loading rate; thereby, slope of infiltration plateau is increased. The reason for the difference between paths of loading and unloading processes is also friction. There is no friction at loading rate of 0.2 m/s; therefore, the unloading process overlaps with the loading process. But difference between loading and unloading processes is increased at loading rates from 0.4 to 1.0 m/s due to increased friction. Since the piston speed at loading and unloading processes is identical in all simulations, the reservoir volume variation is identical in both processes. But, friction in unloading process prevents the defiltration of water molecules from CNT in infiltration plateau. Therefore, density of water molecules in the reservoir and consequently pressure of the

reservoir in unloading process are less than those in loading process.

The required energy for the liquid molecules to adhere to the solid surface is obtained by (Marchand et al. 2011):

$$A_{SL} = \gamma_{SV} + \gamma_{LV} - \gamma_{SL} \quad (4)$$

where γ_{SV} , γ_{LV} and γ_{SL} are solid–vapor, liquid–vapor and solid–liquid surface tensions, respectively. By using Young’s law (Marchand et al. 2011), Eq. 3 can be simplified as follows:

$$A_{SL} - \gamma_{LV} = \gamma_{SV} - \gamma_{SL} = \gamma_{LV} \cos \theta \quad (5)$$

where θ is contact angle. Liquid–vapor surface tensions depend on the interactions between liquid molecules. Since the initial condition of water molecules in reservoir is similar to the bulk water at conditions of 300 K and 1 atm, therefore $\gamma_{LV} = 0.0717 \text{ j/m}^2$ (Vargaftik et al. 1983). The A_{SL} is the interaction energy between the carbon atoms of a CNT and water molecules per the unit area of CNT wall, when the CNT is filled by water molecules. Figure 6 shows values of contact angle at different loading rates in all CNTs. It is observed that the values of contact angle in different loading rates and all CNTs are more than $\pi/2$; therefore, the CNT surface is hydrophobic. So water molecules cannot enter CNT at initial conditions and need an external pressure to infiltrate the CNT. Contact angle and consequently hydrophobicity of CNT are decreased on average 3.6% in all CNTs by increasing loading rate from 0.2 to 1.0 m/s, and thus leading to the decrease of infiltration pressure. Also, contact angle is decreased by increasing the CNT diameter at the same loading rates.

The converted (absorbed) energy in NEAS is given as

$$E = |\Delta\gamma| \times A \quad (6)$$

where $\Delta\gamma = \gamma_{SV} - \gamma_{SL} = A_{SL} - \gamma_{LV}$ and A is the surface area of CNT wall. The absorbed energy density, which is defined as the absorbed energy divided by the total mass of

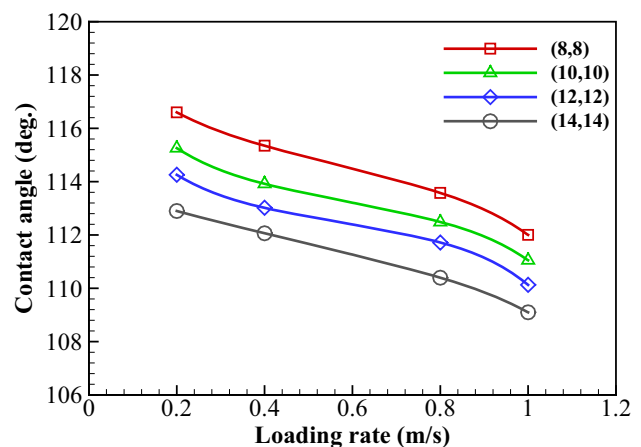


Fig. 6 Contact angle in different loading rates and CNTs

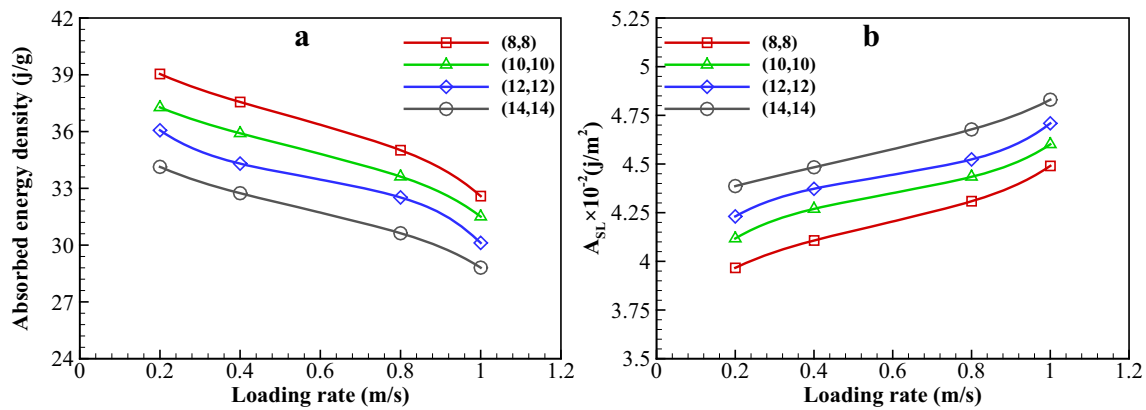


Fig. 7 Variation of **a** absorbed energy density and **b** values of A_{SL} versus loading rate in different CNTs

the carbon atoms of the CNT, and the values of A_{SL} at different loading rates in all CNTs are shown in Fig. 7. The absorbed energy density is decreased on average 16% in all CNTs by increasing loading rate from 0.2 to 1.0 m/s. As shown in Fig. 7a, the absorbed energy density is decreased by increasing the CNT diameter at the same loading rates. Input mechanical energy which is equal to A_{SL} at infiltration stage is converted into two parts:

$$W_{in} = A_{SL} = E_{SL} + E_F \quad (7)$$

where E_{SL} is part of the input mechanical energy that converts into surface tension, and E_F is the other part of the input mechanical energy that overcomes friction. It is observed that $E_F = 0$ at loading rate 0.2 m/s, thus $W_{in} = E_{SL}$. Moreover, as shown in Fig. 7b, E_F is increased by increasing the loading rate and the CNT diameter. Therefore, friction is increased by increasing loading rates and the CNT diameter.

The absorbed energy efficiency is defined as

$$\eta = \frac{|\Delta\gamma|}{A_{SL}} \quad (8)$$

and its values at different loading rates in all CNTs are shown in Fig. 8. It is seen that absorbed energy efficiency is decreased on average 24.8% in all CNTs by increasing loading rates from 0.2 to 1.0 m/s. As shown in Fig. 8, the absorbed energy efficiency is decreased by increasing the CNT diameter at same loading rates.

4 Conclusion

Performance of NEAS under mid-speed loading was investigated by using molecular dynamics simulation, and the effects of tube size were also studied. For this purpose, four loading rates of 0.2, 0.4, 0.8 and 1.0 m/s were applied on the NEAS and four CNTs (8,8), (10,10), (12,12) and (14,14) were selected. The results showed that in loading–

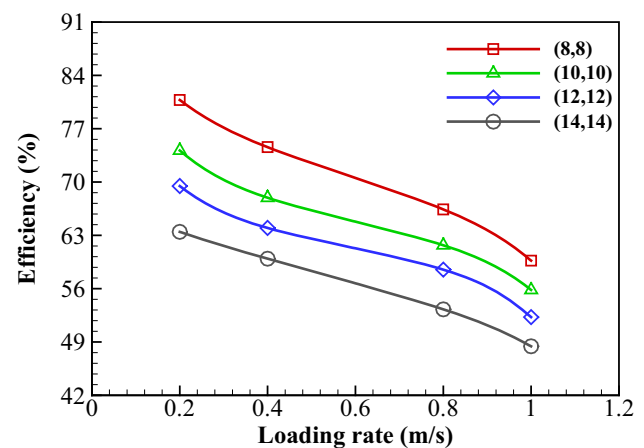


Fig. 8 Variation of absorbed energy efficiency versus loading rate in different CNTs

unloading cycle, slope of infiltration plateau at loading rate 0.2 m/s in all CNTs is zero. Therefore, in all CNTs, there is no friction at loading rate of 0.2 m/s during movement of water molecules in the CNT. But, by increasing the loading rate from 0.2 to 1.0 m/s, slope of infiltration plateau in the infiltration curve in all CNTs is increased. Slope of infiltration plateau in all CNTs at loading rates of 0.4–1.0 m/s is caused by friction. Therefore, friction is increased by increasing loading rates from 0.2 to 1.0 m/s in all CNTs. In addition, friction is increased by increasing the CNT diameter at the same loading rate. This increase of friction causes input mechanical energy to increase. Contact angle which shows the hydrophobicity of CNT is reduced on average 3.6% in all CNTs by increasing the loading rate from 0.2 to 1.0 m/s. As a result, infiltration pressure is decreased on average 41.6% in all CNTs. The absorbed energy density and efficiency of NEAS are decreased on average 16 and 24.8% in all CNTs, respectively. Also, contact angle, infiltration pressure, absorbed energy density and efficiency are decreased by increasing the CNT

diameter at the same loading rate. The effects of chiral vector of CNT on the performance of NEAS will be carried out in the future work of the authors.

References

- Bojan MJ, Steele WA (1987) Interactions of diatomic molecules with graphite. *Langmuir* 3:1123–1127
- Cao G (2012) Working mechanism of nanoporous energy absorption system under high speed loading. *J Phys Chem C* 116:8278–8286
- Cao G, Qiao Y, Zhou Q, Chen X (2008) Water infiltration behaviours in carbon nanotubes under quasi-static and dynamic loading conditions. *Mol Simul* 34:1267–1274
- Chen X, Xu B, Liu L (2014) Nanoscale fluid mechanics and energy conversion. *Appl Mech Rev* 66:050803
- Han A, Qiao Y (2007) Infiltration pressure of a nanoporous liquid spring modified by an electrolyte. *J Mater Res* 22:644–648
- Han A, Kong X, Qiao Y (2006) Pressure induced liquid infiltration in nanopores. *J Appl Phys* 100:014308
- Han A, Punyamurtula VK, Qiao Y (2008) Heat generation associated with pressure-induced infiltration in a nanoporous silica gel. *J Mater Res* 23:1902–1906
- Han A, Lu W, Punyamurtula VK, Kim T, Qiao Y (2009) Temperature variation in liquid infiltration and defiltration in a MCM41. *J Appl Phys* 105:024309
- Hummer G, Rasaiah JC, Noworyta JP (2011) Water conduction through the hydrophobic channel of a carbon nanotube. *Nature* 414:188–190
- Kong X, Qiao Y (2005) Improvement of recoverability of a nanoporous energy absorption system by using chemical admixture. *Appl Phys Lett* 86:151919
- Leach AR (2011) *Molecular modelling, principles and applications*. Prentice Hall, Englewood Cliffs
- Liu H, Cao H (2013) Interaction between mechanical wave and nanoporous energy absorption system. *J Phys Chem C* 117:4245–4252
- Liu H, Cao G (2014) Super energy absorption system based on nanofluidic glycerol solution. *J Phys Chem C* 118:25223–25233
- Liu L, Qiao Y, Chen X (2008) Pressure-driven water infiltration into carbon nanotube: the effect of applied charges. *Appl Phys Lett* 92:101927
- Liu L, Zhao J, Culligan PJ, Qiao Y, Chen X (2009) Thermally responsive fluid behaviors in hydrophobic nanopores. *Langmuir* 25:11862–11868
- Marchand A, Weijts JH, Snoeijer JH, Andreotti B (2011) Why is surface tension a force parallel to the interface. *Am J Phys* 79:999–1008
- Plimpton SJ (1995) Fast parallel algorithms for short-range molecular dynamics. *J Comput Phys* 117:1–19
- Qiao Y, Punyamurtula VK, Xian G, Karbhari VM, Han A (2008) Conversion of mechanical work to interfacial tension in a nanoporous silica gel. *Appl Phys Lett* 92:063109
- Surani FB, Kong X, Panchal DB, Qiao Y (2005) Energy absorption of a nanoporous system subjected to dynamic loadings. *Appl Phys Lett* 87:163111
- Vargaftik NB, Volkov BN, Voljak LD (1983) International tables of the surface tension of water. *J Phys Chem Ref Data* 12:817–820
- Xu B, Qiao Y, Zhou Q, Chen X (2011) Effect of electric field on liquid infiltration into hydrophobic nanopores. *Langmuir* 27:6349–6357
- Xu B, Qiao Y, Chen X (2014) Mitigating impact/blast energy via a novel nanofluidic energy capture mechanism. *J Mech Phys Solids* 62:194–208
- Zhao J, Liu L, Culligan PJ, Chen X (2009) Thermal effect on the dynamic infiltration of water into single-walled carbon nanotubes. *Phys Rev E* 80:061206